2014

A Heuristic Supply Air Temperature Reset Strategy for VAV Systems Employing Variable-Capacity DX Cooling Equipment

Jie Cai
Purdue University, United States of America, cai40@purdue.edu

James E. Braun
Purdue University, United States of America, jbraun@purdue.edu

GENERALIZED HEURISTIC CONTROL FOR DIRECT EXPANSION (DX) COOLING SYSTEMS WITH CAPACITY MODULATION AND VARIABLE AIR FLOW

Jie Cai[1]* and James E. Braun[2]

[1]Ray W. Herrick Laboratory, Purdue University, US
cai40@purdue.edu

[2]Ray W. Herrick Laboratory, Purdue University, US
jbraun@purdue.edu

* Corresponding Author

ABSTRACT

This paper presents a generalized control heuristic to reset supply air temperature setpoints for DX units with capacity modulation and variable air flow. The heuristic is shown to work well for different DX systems with different compressor types and fan-duct combinations. Digital scroll and variable-speed compressors were considered and modeled using curve fits to manufacturer's data. Evaporator and condenser models were also constructed using the catalog data of a representative split DX cooling system. The component models were coupled to provide an overall performance map for each DX system. Fan power is another critical portion of the total HVAC power consumption. In this study, a simple method was used to characterize the performance of a duct system based on typical relationships between pressure drop and air flow rate. Different duct characteristics were coupled to different types of supply fans to provide a set of fan power maps. Optimization was then performed for each combination to find the optimal supply air temperature that minimizes total fan and compressor power. This provided a baseline for developing and validating results of the heuristic control strategy. To assess the integrated energy savings potential of the heuristic strategy, a simulation platform was developed for a medium sized commercial building. Simulations were carried out for a 100-day cooling season in different U.S. locations and under different control strategies, including a conventional control with a constant supply air temperature setpoint and the heuristic reset strategy. It is shown that the heuristic control can provide significant cost savings relative to conventional control depending on the system type and location.

1. INTRODUCTION

Direct expansion (DX) cooling systems are commonly used in small to medium sized commercial buildings due to low capital investment and maintenance cost. Nowadays more DX units are equipped with variable-speed fans and capacity modulating techniques for higher efficiency and better comfort control. This complexity provides greater energy savings potential for control optimization compared to single stage DX units with constant air flow.

Several studies have been found in the literature related to control and optimization of DX cooling systems with capacity modulation and variable airflow. Li et al. (2007) proposed a DDC-based capacity controller for a DX air conditioning system aiming at simultaneous control of indoor dry-bulb temperature and humidity level, using sensible heat ratio (SHR) as a control variable. For the same purpose, Qi et al. (2009) proposed a multi-input-multi-output (MIMO) controller based on a Linear Quadratic Gaussian (LQG) technique which directly controls the compressor and supply fan speeds. Both methods were based on coordinating the control of compressor capacity and supply fan speed to adjust the dehumidifying capability of the DX unit while meeting the required sensible loads. This effect also plays an important role in this study. However, neither of the two papers concerned energy optimization. Vakiloroaya et al. (2011) tried to minimize energy consumption of a DX rooftop package by controlling the refrigerant mass flow rate and supply air temperature. But the paper mainly focused on testing of the proposed optimization technique and did not provide any comprehensive analysis on the source of the energy savings. Andrade and Bullard (2002) studied the effect of different combinations of supply air flow rates and

compressor speeds on the performance of indoor humidity control as well as equipment efficiency for residential air conditioning systems. But it used a third variable, runtime fraction, for optimization and did not consider explicitly the tradeoff between supply fan power and compressor power.

This study was motivated by some optimization results for a 60-ton DX air conditioning system that has reciprocating compressors (unloading-based capacity modulation) and a variable-speed supply fan from a previous study (Cai and Braun, 2013). The results indicate that the system is most efficient when the supply air temperature is at the upper bound. That is because the compressor power dominates the supply fan power, and for a fixed sensible load compressor power decreases significantly with increasing supply air temperature setpoint. Based on this observation, a heuristic control was proposed which increases supply air temperature to the point where it can just satisfy the sensible and latent loads. The control algorithm was tested within simulation for a cooling season and 14% energy savings was predicted.

In this study, a generalized heuristic control for DX units with capacity modulation and variable air volume, is proposed and tested under different system configurations, including different combinations of compressors, fans and duct systems. To make it practical and implementable in real building operations, a simple heuristic logic is developed to dynamically reset the supply air temperature setpoint by monitoring the zone comfort and DX coil status. To test the integrated performance of the proposed heuristic logic, a coupled HVAC-envelope simulation platform was established and used to assess the energy savings potential of the heuristic logic for different climates. Results show that significant energy savings could be achieved but they are influenced by both system configuration and application climate. The generalized heuristic control could have a big impact on the HVAC market since DX type systems represent a significant portion of the current air conditioning systems in the US and the proposed heuristic offers a model-free and, thus, cost-effective alternative for energy efficient control.

It would be helpful to introduce the general idea of the heuristic control here so that the audience could easily understand the role of each section while going through the whole paper. Compressor and supply fan are the two main energy consumers in a DX unit if the condenser fan power is neglected. To provide a fixed sensible cooling capacity, the unit could supply less air with a lower supply air temperature or higher airflow with higher supply air temperature. In general, higher supply air temperature could reduce compressor power (evaporating temperature is higher) and reduce latent load, which leads to a higher sensible COP for the compressor. But higher supply air temperature would increase fan power since more air needs to be delivered. So there is a tradeoff between compressor and fan powers and the heuristic is dedicated to find the balancing point. As will be seen in the following sections, different system configurations put different weights on the two competitors and lead to different energy savings. But the optimal balancing point, or optimal supply air temperature, has a fixed pattern which forms the basis of the proposed heuristic.

2. DX UNITS

2.1 Component Models

Catalog data was downloaded from manufacturer's websites for the evaporator, condensing unit and compressors of the DX unit that is considered in this study (related information are listed in **Table 1**). With linear/nonlinear regression, component models were constructed from the data and these models were coupled to form an integrated model using energy and mass balances. The reasons to adopt this component-based modeling approach are (1) catalog data does not provide part load performance and (2) different types of compressors were considered in this study for the DX units. The evaporator and condenser models are of a gray-box type and are physically-based so that they are able to extrapolate outside the range of catalog data.

2.1.1 Evaporator

The evaporator's catalog data provides total and sensible cooling capacities for different combinations of evaporating temperature (T_{evap}), airflow rate (V) and wet-bulb temperature of air entering evaporator coil ($T_{air,wb,evap}$). But all the data are based on a constant dry-bulb temperature of air entering the evaporator ($T_{air,db,evap}$=80F), and performance at other dry-bulb temperatures is lacking. To facilitate extrapolation to any operating condition, a physically based modeling approach was adopted, which uses an effectiveness-NTU method to calculate the total capacity and a bypass factor method to obtain the sensible capacity. A mathematical description of the gray-box model is given in Equations (1) to (3). The combined heat transfer coefficient (UA) is correlated with airflow rate,

and effectiveness and total capacity are calculated based on the calculated *UA* value. The bypass factor method assumes the leaving air is a mixture of air that bypasses the coil and air that comes into equilibrium with the surface at an apparatus dew point condition. Based on a correlation to airflow rate, the bypass factor can be calculated and sensible capacity can also be obtained. The details of the modeling approach can be found in Cai and Braun (2014). Catalog data with *SHR* lower than 1 was used to train the model and the fitting relative root mean square errors (RMSE) were 3.4% for total capacity and 4.2% for *SHR*. The resulting model has the input-output form shown in Equation (4).

$$q_{tot} = \varepsilon m_{air}(h_{air,in} - h_{air}\left[T = T_{evap}, RH = 1\right]) \tag{1}$$

$$\varepsilon = 1 - e^{(-Ntu)} = 1 - e^{-\frac{UA}{m_{air}}} \tag{2}$$

$$\frac{1}{UA} = \beta_1 (m_{air})^{\beta_2} + \beta_3 \tag{3}$$

$$\left[q_{tot}, q_{sen}\right] = Evap\left(T_{evap}, V, T_{air,db,evap}, T_{air,wb,evap}\right) \tag{4}$$

2.1.2 Compressor

The compressor catalog map is assumed to be valid for a wide range of operating conditions and no extrapolation is needed. Thus, it can be used directly to calculate compressor performance. The model form is shown in Equation (5) and this form is used for both power consumption and refrigerant mass flow rate with coefficient sets that are provided by the compressor manufacturers for each stage of control. Two types of compressors are considered in this study: digital scroll and variable-speed compressors. One representative compressor was selected for each type but both models follow the same input-output form as shown in Equation (6). The variable *Stage* is a continuous variable from 0 to 1 representing either the run-time fraction for a digital scroll compressor or the speed ratio for a variable-speed compressor. Since the catalog data only provides coefficient sets for several discrete *Stage* values, the model in Equation (6) only admits the *Stage* values that are available. As will be discussed in a later section, a meta-model was trained using data generated by a detailed integrated model. The training data were calculated with *Stage* values corresponding to the catalog data that was directly available. The meta-model then allowed interpolation/extrapolation to other *Stage* values, which was not necessary for the component-based model.

.

$$\begin{aligned} Y = {} & c_0 + c_1 T_{evap} + c_2 T_{cond} + c_3 T_{evap}^2 + c_4 T_{evap} T_{cond} + c_5 T_{cond}^2 + c_6 T_{evap}^3 + c_7 T_{evap}^2 T_{cond} \\ & + c_8 T_{evap} T_{cond}^2 + c_9 T_{cond}^3 \end{aligned} \tag{5}$$

$$\left[P_{comp}, m_r\right] = Compressor\left(T_{evap}, T_{cond}, Stage\right) \tag{6}$$

The digital scroll compressor that was selected is a dual-compressor set with one standard scroll compressor and one digital scroll compressor. The digital scroll takes the lead, so for *Stage* between 0 and 0.5, the standard compressor is off and the digital scroll modulates through high-frequency unloading. For *Stage* between 0.5 and 1, the standard compressor is on and provides 50% of the total capacity while the digital scroll is responsible for the rest. For example, when *Stage* = 0.7, the digital compressor will modulate with a 0.4 run-time fraction (providing 20% of the total capacity), and the standard compressor is turned on (providing 50% of the total capacity). Catalog data provides information at 50% and 100% part load ratios for each of the two compressors, so the compressor set has performance directly available at 25%, 50%, 75% and 100% part load ratios.

The authors had no luck in finding a variable speed compressor that has accessible catalog data for the same capacity as the digital scroll. Instead, a 2.65-ton variable-speed compressor was chosen and the performance was scaled accordingly. For the variable-speed compressor, *Stage* corresponds to the speed ratio of the compressor motor. The catalog data is available at part load ratios from 25% to 100% with a 2% increment.

2.1.2 Condenser

There is no catalog data directly available for the condensing coil. This study inferred its performance based on the catalog maps of other components. A condensing unit that is configured with a 30-ton digital scroll compressor set (the same digital scroll compressor discussed above) was chosen and the unit catalog data was downloaded from the manufacturer's website. A quadratic fit for the condensing unit capacity was obtained with the input-output form shown in Equation (7). By equating the evaporator's total cooling capacities (q_{tot}) in Equations (4) and (7), the evaporating temperature (T_{evap}) was obtained given other input variable values. Then the compressor model in Equation (6) was used to solve for the condensing temperature (T_{cond}) to get a 15 F subcooling. In the iterative process, the compressor was assumed to have a 5% heat loss fraction and the condenser refrigerant outlet condition was obtained using mass and energy balances. The condensing unit catalog data corresponds to full capacity operation, so in the calculation *Stage* was set to 1 in Equation (6). Once the condensing temperature and condenser capacity were obtained, the condenser effectiveness model shown in Equations (8) to (10) was trained. It was assumed that the air flow rate across the condensing coil ($m_{cond,air}$) is constant and it is a parameter that needs to be estimated in the training process along with the other parameters (α_1 to α_3). The estimated condensing coil model has the input-output form shown in Equation (11).

$$q_{tot} = CondUnit(T_{evap}, T_{amb}) \tag{7}$$

$$q_{cond} = \varepsilon m_{cond,air}(T_{amb} - T_{cond}) \tag{8}$$

$$\varepsilon = 1 - e^{(-Ntu)} = 1 - e^{-\frac{UA}{m_{cond,air}}} \tag{9}$$

$$\frac{1}{UA} = \alpha_1 (m_r)^{\alpha_2} + \alpha_3 \tag{10}$$

$$q_{cond} = Cond(T_{cond}, T_{amb}, m_r) \tag{11}$$

Table 1: Type and Capacities of Components Obtained from Manufacturers' Information

	Type	**Capacity**
Evaporator	Standard DX coil	30 tons
Compressor	Standard scroll	15 tons
	Digital scroll	15 tons
	Variable speed	2.65 tons
Condensing unit	Air-cooled CU	30 tons

2.2 Integrated Model

Table 2 shows the input-output correspondence for the three main components that were presented. They are just repetitions of Equations (4), (6) and (11) but they mark out different types of input variables. The single-underscored variables are external inputs (evaporator inlet air condition, outdoor air temperature, compressor stage number and supply air flow rate) while the double-underscored variables (evaporating and condensing temperatures) are internal variables that need to be solved iteratively by satisfying the two equations shown in Equation (12). The integrated model has an input-output form shown in Equation (13).

$$\begin{cases} q_{tot} + 0.95 \times P_{comp} = q_{cond} \\ T_{sc} = 15 \text{ F} \end{cases} \tag{12}$$

$$\left[P_{comp}, q_{tot}, SHR, T_{sup} \right] = DX(T_{air,db,evap}, T_{air,wb,evap}, T_{amb}, V, Stage) \tag{13}$$

Table 2: Model input-output forms for the main components

	Model input-output form
Evaporator	$[q_{tot}, q_{sen}] = Evap\left(\underline{\underline{T_{evap}}}, \underline{V}, \underline{T_{air,db,evap}}, \underline{T_{air,wb,evap}}\right)$
Compressor	$\left[P_{comp}, m_r\right] = Compressor\left(\underline{\underline{T_{evap}}}, \underline{\underline{T_{cond}}}, \underline{Stage}\right)$
Condenser	$q_{cond} = Cond(\underline{\underline{T_{cond}}}, \underline{T_{amb}}, m_r)$

Figure 1 shows the variation of some key outputs with respect to the normalized *Stage* or part load ratio for the integrated models with variable-speed and digital scroll compressors. The trends are similar between the two units for most of the plotted variables. With increasing *Stage* value, the temperature or pressure lift from the evaporator to the condenser increases and energy equilibrium drives the evaporating temperature to decrease and the condensing temperature to increase. Because of the lower evaporating temperature, more dehumidification occurs and *SHR* decreases with higher *Stage* value. Cycle efficiency increases monotonically from full-load conditions with decreasing *Stage* value because of the lower temperature lift. However, part load degradation of the compressor can counter the effect of decreasing lift and can lead to a peak efficiency at a balancing point between the two effects. Digital scroll compressors have significant compressor part load degradations so the COP plot has a peak efficiency at a *Stage* value close to 0.55. Decreasing the *Stage* value below this point leads to significant performance degradation. Some experimental results from other researchers exhibit this behavior for systems with digital scroll compressors, such as results presented by Zhang et al. (2011). For variable-speed compressors, the compressor part load degradation is much less significant and, as a consequence, unit efficiency increases monotonically as *Stage* value decreases within its practical range of operation, which can be seen in the COP plot in **Figure 1**. This type of behavior for variable-speed compressors can also be found in previous research such as presented by Park et al. (2001). The different behavior of efficiency with respect to changing part load ratio leads to different energy savings opportunities, as will be discussed in the following sections.

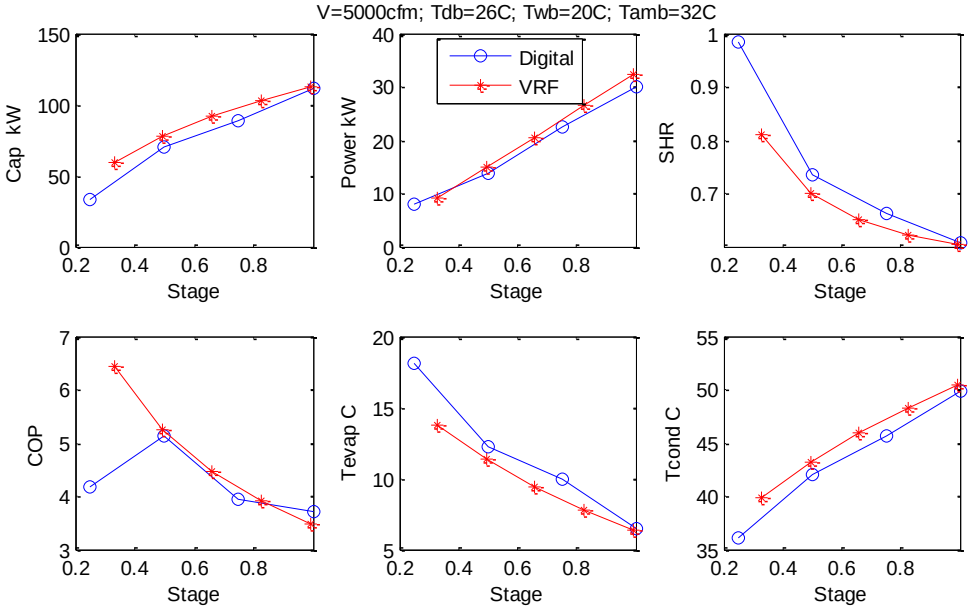

Figure 1: Integrated performances of DX units with digital scroll and variable-speed compressors

Figure 2 shows the variation of COP and SHR with respect to changes of different inputs for the two integrated models. It can be seen that trends are similar between the two models. COP decreases significantly with higher outdoor air temperature as a result of higher condensing temperature and larger temperature lift from evaporator to condenser. However, ambient temperature does not significantly affect evaporating temperature so the SHR is

relatively constant with different ambient temperatures. With fixed dry-bulb temperature but higher web-bulb temperature, the mixed air has higher humidity and more dehumidification occurs on the DX coil. Thus, SHR decreases dramatically with increasing web-bulb temperature. With higher airflow rate, the evaporating temperature increases which leads to higher SHR. COP increases slightly with higher airflow rate or web-bulb temperature as a result of small increase on evaporating temperature.

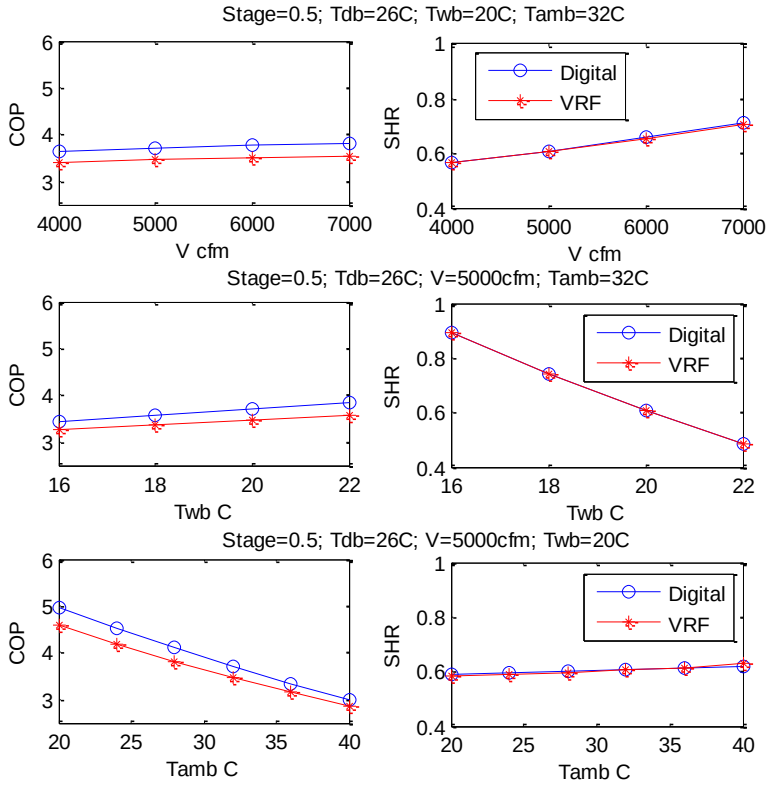

Figure 2: Variation of COP and SHR with respect to changes of different inputs for DX units with digital scroll and variable-speed compressors

2.3 Meta-Model

The integrated model requires an iterative solution for the evaporating and condensing temperatures in order to determine cooling capacity and compressor power. As a result, the model involves significant computation and is not suitable for direct use in optimization. To overcome this problem, an empirical meta-model was developed that directly correlates total capacity and power consumption using the form of Equation (14). Training data over a wide range of operating conditions was generated with the integrated model and used to estimate the coefficients. Linear regression was used to estimate the combined coefficients after expanding the right hand side of Equation (14). The *SHR* calculation uses the bypass factor model and the meta-model input-output form remains the same as shown in Equation (13).

$$q_{tot}(P_{comp}) = \left(a_0 + a_1 T_{air,wb,evap} + a_2 T_{air,wb,evap}^2 + a_3 T_{amb} + a_4 T_{amb}^2 + a_5 T_{air,wb,evap} T_{amb}\right) \cdot \left(b_0 + b_1 V + b_2 V^2\right)\left(c_0 + c_1 Stage + c_2 Stage^2\right) \quad (14)$$

3. FAN-DUCT SYSTEMS

The supply fan power consumption is mainly dependent on building loads, duct system characteristics and the type of fan that is being used. In this section, three types of commonly used supply fans are considered. Duct resistance is

characterized under both constant static pressure and static pressure reset controls. The fan power curves are compared for different combinations.

3.1 Duct System Characteristics

The characteristics of a ductwork system determine the pressure drop across the air distribution system and also the fan power consumption. **Figure 3** depicts the critical pressures in an air distribution system and the pressures can be related by the following equations (Wang, 1998)

$$ESP = \Delta P_{fan,downstream} + \Delta P_{fan,upstream}$$
$$\Delta P_{fan,downstream} = P_{sup} - P_{zone} = A \cdot V^2$$
$$\Delta P_{fan,upstream} = P_{zone} - P_{fan,inlet} = B \cdot V^2$$

where ESP is the external static pressure rise of the fan, $\Delta P_{fan,downstream}$ is the pressure drop across the ductwork that is downstream of the fan including the supply ducts and VAV damper , and $\Delta P_{fan,upstream}$ represents the pressure drop upstream of the supply fan from the building space. B is the total upstream friction loss coefficient, which could be assumed constant if the mixed and return damper openings do not vary significantly. The value of the downstream friction loss coefficient, A, is mostly dependent on the VAV damper openings and is hard to obtain for systems with multiple VAV boxes. However, under the aforementioned two static pressure control strategies, the pressure calculation can be simplified. Under constant static pressure control, ESP can be obtained via Equation (15), where $\Delta P_{fan,downstream}$ is a constant since P_{sup} is controlled to the setpoint value and P_{zone} does not change much. For systems with static pressure reset, Equation (16) can be used to calculate ESP in which the friction coefficient A is assumed to be constant. That is because there is always at least one VAV box with a fully opened damper and the VAV damper openings are relatively stationary if the load distribution to the zones does not vary much with time.

$$ESP = \Delta P_{fan,downstream} + \Delta P_{fan,upstream} = D + A \cdot V^2 \quad (15)$$

$$ESP = \Delta P_{fan,downstream} + \Delta P_{fan,upstream} = (A + B) \cdot V^2 = C \cdot V^2 \quad (16)$$

To test the validity of the two model forms, field data was collected from a building, the model of which is discussed in the simulation section. The building was controlled with a constant static pressure during 2012 and the system was retrofitted in 2013 to have resetting static pressures. Two data sets corresponding to the two different controls were obtained and used to fit the two models, and the results are shown in **Figure 4** and **Figure 5**. It can be seen that the constant static pressure setpoint was 1.4 in W.C. after offsetting the space pressure during the year of 2012. The corresponding data fits well with the proposed model form. The pressure resetting data has a large variance due to the unsynchronized damper openings between the VAV boxes. However, the model is still able to capture the trend and provide an approximate correlation between the pressure and airflow.

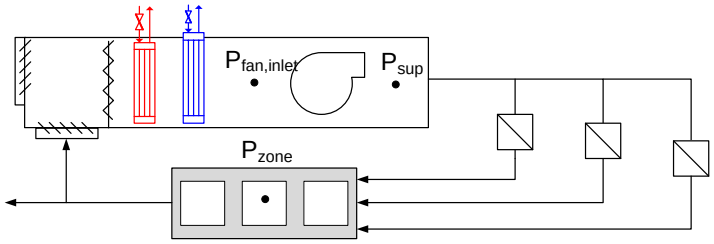

Figure 3: Critical pressures in a duct system

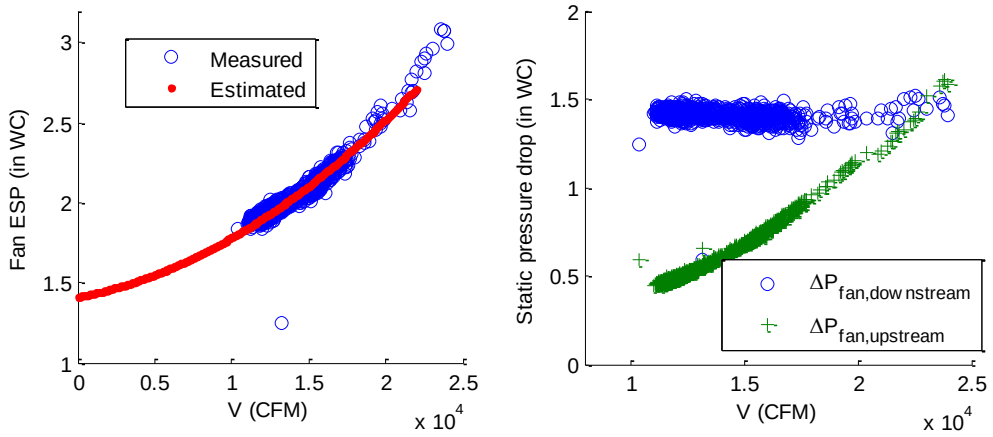

Figure 4: *ESP* estimation with constant static pressure control

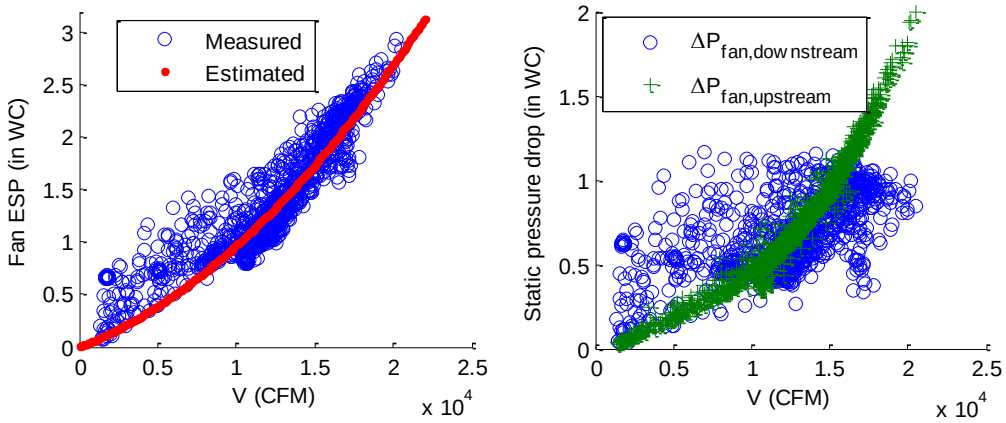

Figure 5: *ESP* estimation with resetting static pressure control

3.2 Fans

Three types of fans are considered in this study: forward-curved (FC), airfoil (AF) and vaneaxial (Q) fans. One representative has been chosen for each type and the corresponding performance data was downloaded from the manufacturer's website. The model numbers and some key parameters of the selected fans are listed in **Table 3**.

Table 3: Key parameters for the selected fans

	Diameter (in)	**Maximum SP (in wc)**	**Maximum HP (bhp)**
FC (forward curved)	25	5	30
AF (airfoil)	22	8	40
Q (vaneaxial)	36.5	5	30

A quadratic form is used to correlate the fan power to the fan static pressure and airflow rate. Correlation coefficients were estimated via data fitting with the performance data for each of the models. The maximum fitting errors are 3% for the FC and Q fans and 5% for the AF fan.

3.3 Fan power curve

Combining the duct system characteristics with the fan power maps, the fan power consumption can be calculated given the total air flow rate for a specific fan-duct system. Equation (17) shows the fan power model, which firstly determines the external static pressure for a given airflow rate based on the duct pressure model and then uses the fitted fan map to calculate the fan power consumption. **Figure 6** plots the power consumptions for different types of fans under resetting and constant static pressure controls, with the static pressures calculated based on the fitted

pressure models in the preceding section. It can be observed that the Q fan and the FC fan have similar performances but the AF fan consumes more power than the other two at the same airflow rate. Also static pressure reset control leads to a steeper slope compared to constant static pressure control for all the fan curves. As a consequence, both the fan type and pressure control scheme will have an impact on the energy savings of the heuristic control strategy, as will be illustrated in a later section.

$$P_{fan} = FanMap(ESP(V), V) = Power_{fan}(\mathrm{V}) \tag{17}$$

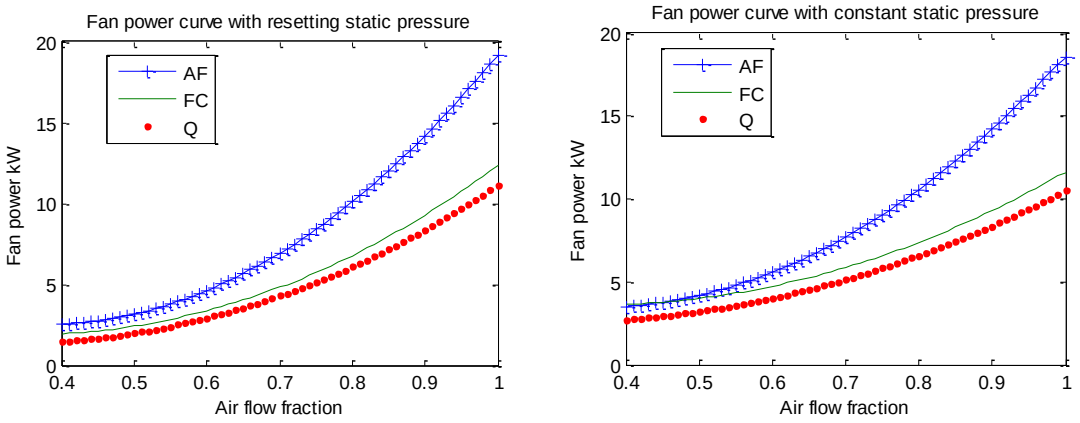

Figure 6: Different fan power consumptions under resetting (left) and constant (right) static pressure control

4. OPTIMAL OPERATIONS

4.1 Problem Formulation

Stage is not directly monitored or controlled in practice. Instead, the compressor stage number is modulated by a feedback controller to maintain a supply air temperature setpoint. Thus, it is more sensible to have a model taking T_{sup} as an input. With the DX unit model, the compressor stage number can be solved iteratively for any supply air temperature leading to a model form shown in Equation (18). It is the same as Equation (13), but with *Stage* and T_{sup} swapped.

$$\left[P_{comp}, q_{tot}, SHR, Stage\right] = DX(T_{air,db,evap}, T_{air,wb,evap}, T_{amb}, V, T_{sup}) \tag{18}$$

To meet a given sensible cooling load, supply air temperature setpoint is the only optimization variable and supply air flow rate is an dependent variable that is determined to meet the load. Thus, the optimization problem can be formulated as follows:

$$T_{sup,opti} = \arg\min_{T_{sup}} P_{DX}\left(\overline{T_{air,db,evap}, T_{air,wb,evap}, T_{amb}}, V, T_{sup}\right) + P_{fan}(V)$$

$$\text{satisfying} \begin{cases} q_{tot} \times SHR = \overline{q_{sen,req}} \\ SHR < \overline{SHR_{\max}} \\ V_{\min} < \dot{V} < V_{\max} \\ Stage \in [0,1] \\ T_{\min} < T_{sup} < T_{\max} \end{cases}$$

In this formulation, the overlined variables are the ambient conditions and sensible/latent load requirement that are specified as inputs. SHR_{max} is the allowed maximum sensible heat ratio, which corresponds to a minimum

dehumidification level. For this specific system, V_{max}=20500cfm and V_{min}= V_{max}/2. The supply air temperature setpoint T_{sup} is the optimization variable and supply airflow rate V is an internal variable.

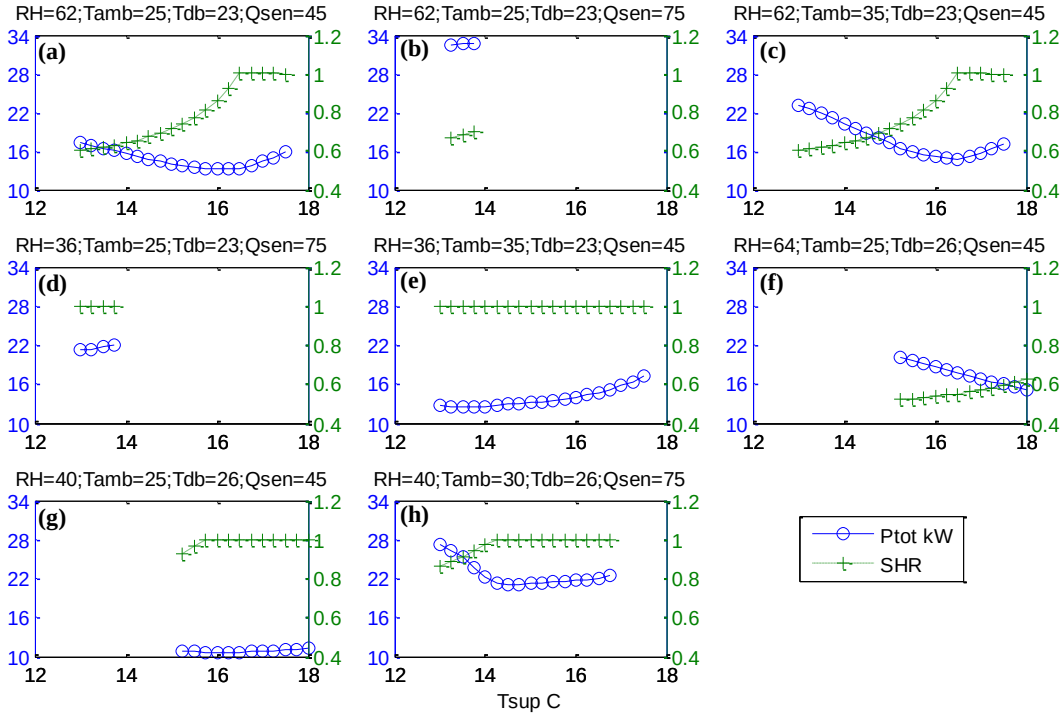

Figure 7: Variation of total power consumption (left-axis label) and SHR (right-axis label) with supply air temperature under different operating conditions for DX unit with digital scroll compressor. *RH* and *Tdb*: air relative humidity (%) and dry-bulb temperature (C) entering evaporator; *Qsen*: required sensible capacity (kW) on DX coil; *Tamb*: ambient temperature (C).

4.2 Optimal Results

Figure 7 plots the variation of total power consumption and *SHR* of the DX unit with respect to supply air temperatures under different operating conditions. The performance was evaluated under the configuration of digital scroll compressor, FC fan and resetting static pressure control. A key observation from the plots is: ***the system is most efficient when the coil condition changes from wet to dry***. Based on this observation, a heuristic strategy is proposed for near-optimal control of DX units: ***the supply air temperature setpoint should be increased until a SHR upper bound is reached.*** If there is a dehumidification requirement, then the *SHR* upper bound takes a value less than 1 depending on the requirement. If not, the *SHR* upper bound is 1 and the heuristic should set the supply air temperature to the lowest value where *SHR* equals 1. Some other observations worth mentioning are:

- (Effect of ambient temperature) Comparison between subplots (a) and (c) shows that for higher outdoor air temperatures, the slope of the total power curve is steeper for the portion of *SHR<1,* and energy saving potential is higher. This is because when the ambient temperature is high, the refrigeration cycle has low efficiency and compressor power strongly dominates the fan power.

- (Effect of mixed air humidity) Comparison between subplots (c) and (e) indicates that when the mixed air is sufficiently dry such that no moisture condenses on the DX coil then the unit is most efficient at the lowest supply air temperature; for humid mixed air when *SHR* is less than one then the DX unit is more efficient with higher supply air temperature.

- (Effect of mixed air humidity) Comparison between subplots (b) and (d) shows that humid mixed air consumes more power to achieve the same sensible cooling load due to the existence of latent load.

- When the required sensible cooling load is high, the feasible supply air temperatures would fall within a narrow range (e.g., subplots (b) and (d)) due to the capacity of airflow. When the required sensible cooling is low and mixed air temperature is high, the supply air temperature cannot go too low due to the lower bound on air flow rate. Under this situation, reheating may be needed for local zone temperature control when the local cooling load is small.

Figure 8 provides performance plots for the DX unit with the variable speed compressor. The trends and conclusions are similar to those associated with the results of **Figure 7**.

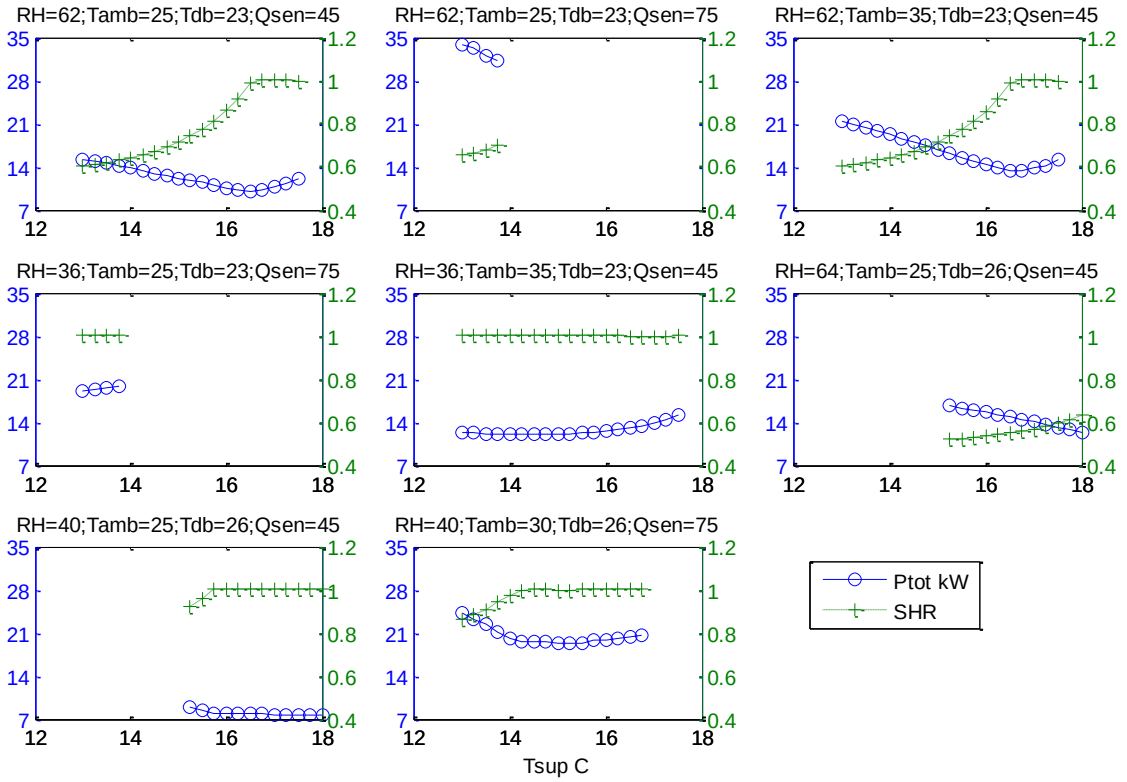

Figure 8: Variation of total power consumption (left-axis label)) and SHR (right-axis label) with supply air temperature under different operating conditions for DX unit with variable speed compressor. *RH* and *Tdb*: air relative humidity (%) and dry-bulb temperature (C) entering evaporator; *Qsen*: required sensible capacity (kW) on DX coil; *Tamb*: ambient temperature (C).

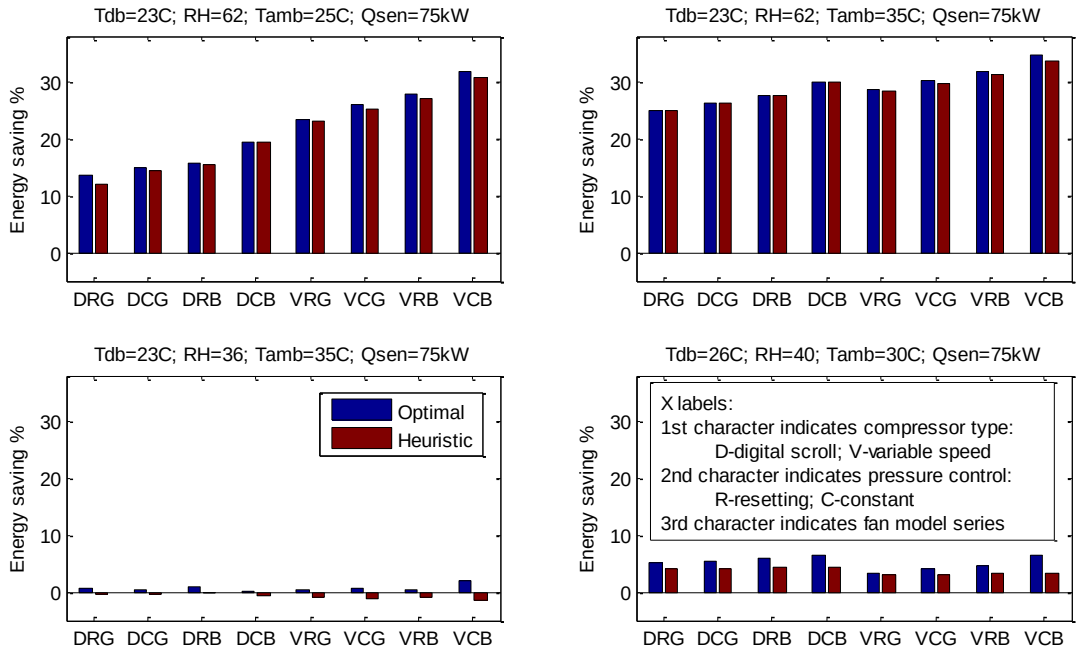

Figure 9: Energy savings of optimal and heuristic controls for different operating conditions under different DX configuration. Baseline T_{sup} = 14C.

4.3 Energy Savings for Different Configurations

The energy savings potential of the proposed heuristic strategy depends on the system configuration and operating conditions. Eight combinations of components were considered in this study and each combination is indexed by a three-character string. The 1st character represents the compressor type (D for digital scroll and V for variable speed). The 2nd character indicates the static pressure control scheme (R for resetting and C for constant supply pressure) and the 3rd character corresponds to the fan type (B for forward curved and G for airfoil). The bar plots in **Figure 9** show the energy savings that were estimated for the optimal and heuristically determined supply air temperatures for different DX unit configurations, compared to a baseline supply air temperature setpoint for 14 C. Each plot corresponds to a specific operating condition; these operating conditions are the same as the conditions in subplots (a), (c), (e) and (h) of **Figure 7**. Some key observations and conclusions are:

- The energy savings for the heuristic control are very close to those achieved with optimal supply air temperatures under all the considered operating conditions.
- In general, the optimal and heuristic control lead to higher energy savings for systems with variable speed compressors than those with digital scroll compressors. That is because the variable speed compressor has better part-load operation and part of the savings opportunity is associated reducing the compressor loading through supply air temperature setpoint adjustments.
- The energy savings associated with optimal and heuristic supply air temperature setpoints are less when static pressure reset is employed compared to a constant static pressure. This is because the sensitivity of fan power (see Section 3.3) to flow is greater for static pressure reset than for fixed static pressure. A greater sensitivity means a greater fan power penalty associated with increasing the supply air temperature set point for a given zone load. For the same reason, the B series (forward curved) fan leads to higher energy savings than the G series (airfoil) fan.
- For the operating condition with RH = 0.4 and Tamb = 30C (right-bottom plot), energy savings potential is small since the baseline supply air temperature is close to optimal (see subplot (h) of **Figure 7**).
- For the condition with RH = 0.36 (left-bottom plot), there is little to no energy savings potential since the DX coil is dry for all feasible supply air temperatures and the total power curve is flat over a wide range (see subplot (h) of **Figure 7**).

5. ENERGY SAVING ASSESSMENT WITH SIMULATION

5.1 Simulation Platform

In order to evaluate seasonal savings potential for the heuristic control, an inverse model was developed for a portion of a medium-sized commercial building from measured data collected in 2013. The details of the model can be found in Cai and Braun (SSB, 2014). The north end of the building is served by a single air handling unit and a 60-ton DX unit. There are 9 VAV boxes conditioning 9 thermal zones and the layout is depicted in **Figure 10**.

In the simulation, all the zones were controlled with a night setup strategy with setpoints of 23C during occupied hours and 25C during unoccupied hours. The simulation time-step was chosen to be 1 hour and perfect feedback control was assumed for the HVAC systems. The simulation was run for a 100-day cooling season and TMY2 data was used as external weather excitations.

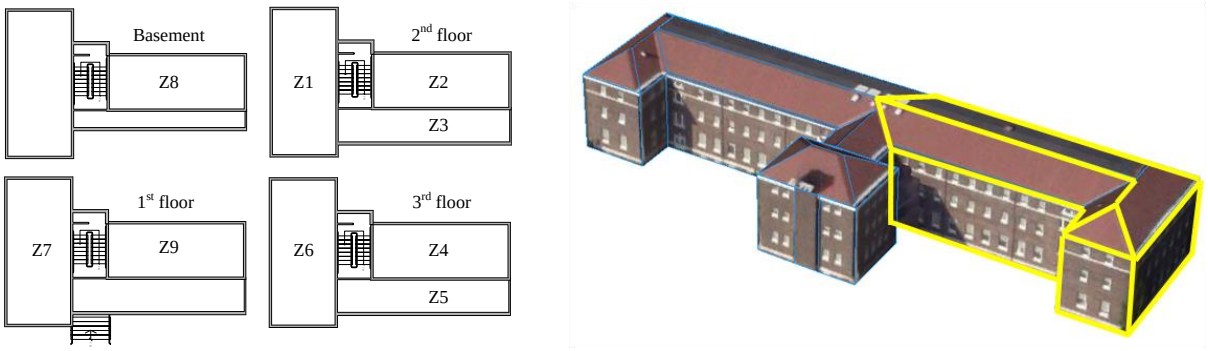

Figure 10: Floor layout and external view of case study building

To evaluate the impact of different climates on the energy savings potential of the proposed heuristic logic, simulations were run with weather data for four different locations of the US. **Figure 11** (taken from PNNL & ORNL, 2010) shows the four locations of Phoenix (AZ), Miami (FL), Madison (WI) and Philadelphia (PA) that were chosen to be representative of hot-dry, hot-humid, cold and mixed-humid climate zones.

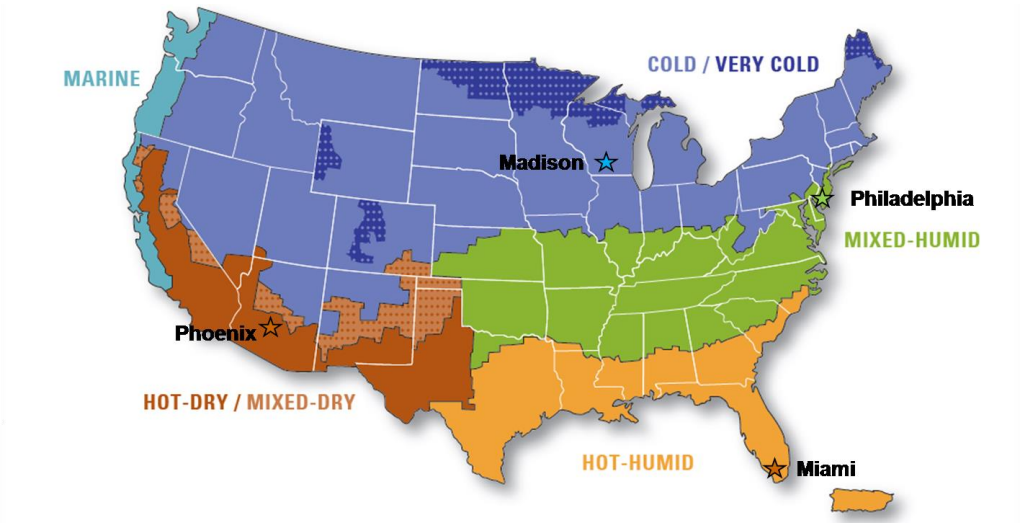

Figure 11: US climate zones and cities chosen to investigate climate impacts on heuristic control savings

5.2 Heuristic Logics

Figure 12 illustrates the heuristic control logic used in the simulation. This logic is based on the heuristic that has been developed in Section 4 and could be implementable in real building operations. This heuristic essentially tries to increase the supply air temperature setpoints whenever possible to enhance the DX unit's efficiency. Three conditions need to be checked at each decision step to determine if an increase in the setpoint should be allowed. The first two conditions concern zone comfort because the supply air temperature must be low enough to satisfy the zone sensible and latent loads. The third condition is related to tracking the transition from a wet to a dry DX coil. When the coil is dry, DX unit efficiency decreases with increasing supply air temperature which is opposite to the trend for a wet coil. Therefore, the goal is to run the coil on the boundary of the wet/dry transition as long the zone temperature and humidity are maintained. As a benchmark, conventional logic with a constant supply air temperature (14 C) was also simulated and used to assess the energy savings potential. This logic was implemented in the building before 2013.

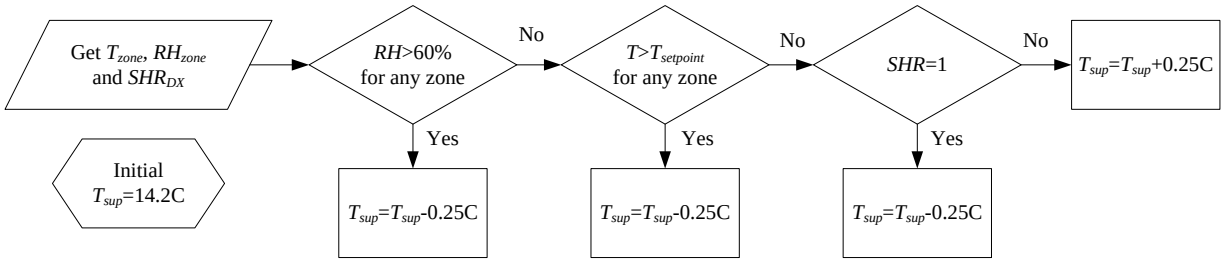

Figure 12: Generalized control heuristics for DX unit

5.3 Simulation Results

Table 4 lists the integrated loads, energy consumption and space humidity (averaged) for the two control strategies at different locations. Estimated cooling season energy savings are 9.3%, 8.5%, 2.9% and 4.8% for Madison, Philadelphia (PHL), Miami and Phoenix, respectively. Most of the time, the heuristic strategy leads to higher supply air temperature and supply air flow rates than the conventional strategy for all four cases, which increases ventilation flows and loads for hot climates (Miami and Phoenix) and decreases ventilation loads for relatively cool places (PHL and Madison). Miami has the least energy savings because the indoor humidity is already high (53%) under the conventional control and there is not much room to optimize due to the 60% upper bound for indoor humidity. Still, the heuristic strategy leads to slightly higher indoor humidity (57%) than the conventional strategy. Energy savings are significant for Madison and Philadelphia. Simulation results for a typical day in Philadelphia are plotted in **Figure 13** on the left. It can be seen from the plots that during unoccupied hours, the heuristic strategy tries to increase the supply air temperature to reduce energy consumption. No dehumidification occurs and space humidity builds up. At 5:00am space humidity reaches the upper bound and supply air temperature is decreased to start dehumidification. At 9:00am the occupied mode is triggered and supply air temperature is further decreased to meet the building sensible loads. More aggressive dehumidification occurs and the space humidity is brought down. The accumulated moisture in the evening is removed during the day time so more power is consumed in the occupied period. However, this is well compensated by the energy savings during the unoccupied period, and a net savings of 9.3% is achieved for the whole cooling season. Similar behavior occurred in Madison. Phoenix has a totally different behavior due to the dry outdoor air conditions and the results are plotted on the right in **Figure 13**. It can be seen that for this specific day, indoor humidity is far below the upper bound so the supply air temperatures are mainly determined by the sensible loads. Slight dehumidification occurs with the conventional control during the evening time and that provides some energy saving with the heuristic strategy. Around 3:00 pm, the supply air temperature determined by the heuristic strategy is lower than the conventional setpoint. In that period, the conventional supply air temperature is not able to satisfy the sensible loads for some of the zones since the airflow rates reach the upper bounds, which cause the temperatures of those zones to go beyond the setpoint. However, the heuristic strategy reduces the supply air temperatures to satisfy the loads of all zones. Therefore, in addition to energy savings, the heuristic strategy also improves indoor comfort.

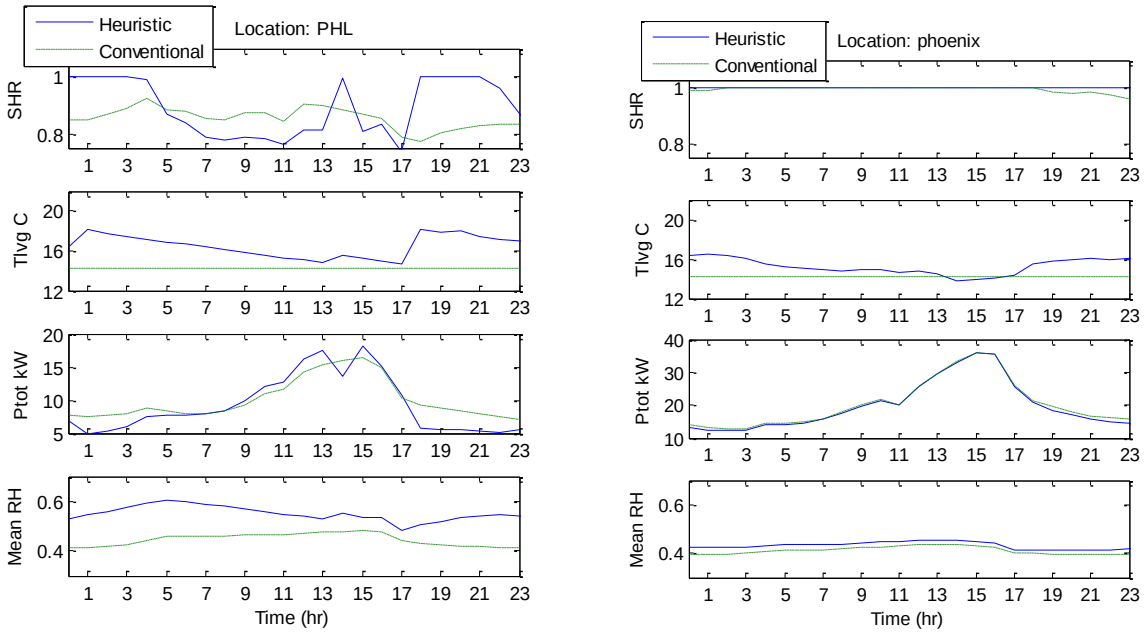

Figure 13: Simulation results under conventional and heuristic controls PHL and Phoenix

Table 4: Some integrated performance comparisons between conventional and heuristic controls

	Qsen on DX coil (MWh)		**Qlatent on DX coil (MWh)**		**Energy consumption (MWh)**		**Mean zone RH %**	
	Heur.	Conv.	Heur.	Conv.	Heur.	Conv.	Heur.	Conv.
Philadelphia	130.1	130.4	15	17.5	25.8	27.5	53	45
Miami	143	142.6	31.1	31.4	35.5	36.5	57	53
Phoenix	173.1	172.7	7.75	11.9	46.5	48.8	52	47
Madison	120.5	122.1	8.3	10.5	22.5	24.8	55	48

6. CONCLUSION

This paper developed a gray-box modeling approach for DX units that is trained using catalog data accessible from manufacturer's websites. Integrated models were developed and demonstrated for two cases: one having a digital scroll compressor and the other with a variable-speed compressor. These physically-based models are able to calculate the unit performance under part load operating conditions, which is not directly available in the catalog maps. Then, inverse duct and fan system models and results were presented for two types of fan control (constant and static pressure reset controls) and for different types of fans. Optimization was then applied to a coupled DX-fan model to determine optimal supply air temperatures given sensible and latent load requirements. The optimal results indicate that the system is most efficient at the point where the DX coil condition changes from wet to dry. Based on this observation, a control heuristic was proposed which finds the supply air temperature at the transition where *SHR* reaches one. The heuristic was evaluated in simulation for the different compressor, fan and static pressure control combinations under different operating conditions and performance was shown to be very close to optimal under all scenarios. Compared to a constant supply air temperature setpoint, significant energy savings potential can be achieved depending on the system configuration as well as the operating condition. The variable-speed compressor was found to be superior to the digital scroll compressor due to its better performance at part load conditions.

To assess the integrated performance of the proposed heuristics, a simulation platform was established which incorporates a data-driven envelope model for a building located at Philadelphia, PA. Simulations were carried out for different climates to evaluate the impact of climate on the performance of the heuristic control logic. It was found that under moderate-humid climates, the heuristic strategy could provide significant energy savings (close to

10%). For hot-dry climates, the energy savings are lower (around 5%) since there is a lower demand for dehumidification. For hot-humid climates, the energy savings are minimal because indoor humidity is already close to the allowed upper bound and there is not much room to optimize.

REFERENCE

1. Qi, Q. and Deng, S., "Multivariable control of indoor air temperature and humidity in a direct expansion (DX) air conditioning (A/C) system". *Building and Environment*, 2009
2. Li, Z. and Deng, S., "A DDC-based capacity controller of a direct expansion (DX) air conditioning (A/C) unit for simultaneous indoor air temperature and humidity control-Part 1: Control algorithms and preliminary controllability tests", *International Journal of Refrigeration*, 2007
3. Vakiloroaya, V., Zhu, J.G. and Ha, Q.P., "Modelling and optimisation of direct expansion air conditioning system for commercial building energy saving", *Proceedings of the 28th International Symposium on Automation and Robotics in Construction*, 2011
4. Andrade, M. A. and Bullard, C. W., "Modulating blower and compressor capacities for efficient comfort control", *ASHRAE Transactions*, 2002
5. Zhang, D., Zhang, X. and Liu, J., "Experimental study of performance of digital variable multiple air conditioning system under part load conditions", *Energy and Buildings*, 2011
6. Park, Y.C., Kim, Y.C. and Min, M.K., "Performance analysis on a multi-type inverter air conditioner", *Energy Conversion and Management*, 2001
7. Putta, V., Cai, J., Kim, D., Braun, J. E. and Hu, J., "Simulation Based Assessment of Alternative Approaches for Model Predictive Control in Multi-Zone Buildings", *International Conference for Enhanced Building Operations*, 2014, to appear
8. Wang, S. and Burnett, J., "Variable-air-volume air-conditioning systems: Optimal reset of static pressure setpoint", *Building Services Engineering Research & Technology*, 1998
9. Trane, "Fan performance data for Central-Station Air Handlers", http://www.trane.com/content/dam/Trane/Commercial/global/products-systems/equipment/terminal-devices/ventilation-fans/clch-prc008-en.pdf, 2004
10. Cai, J. and Braun, J.E., "Development and Assessment of Heuristic Control Strategies for a Multi-Zone Commercial Building Employing a Direct Expansion System" (presentation) *Intelligent Building Operations Workshop, Boulder*, 2013, presentation accessible at: http://www.ibpsa.us/presentations/2013.06_IBO_Boulder/Friday/Optimal%20Control%20Approaches%20and%20Results%20II/OptimalControlII_JieCai_final.pdf
11. Cai, J. and Braun, J.E., "Gray-box modeling of multi-stage direct-expansion (DX) to enable control system optimization", *ASHRAE Transactions*, 2014, submitted
12. Cai, J. and Braun, J.E., "A practical and scalable inverse modeling approach for multi-zone buildings", *9th International Conference on System Simulation in Buildings*, 2014, to appear
13. PNNL & ORNL, High-Performance Home Technologies: Guide to Determining Climate Regions by County, 2010

ACKNOWLEDGEMENT

This work was supported by the Department of Energy through the Energy Efficient Buildings Hub (renamed as the Consortium for Building Energy Innovation).

NOMENCLATURE

A,B = friction loss coefficient
ESP = external static pressure
$\Delta P_{fan,upstream}$ = fan upstream pressure loss
$P_{fan,inlet}$ = pressure at fan inlet
P_{sup} = supply duct pressure
$\Delta P_{fan,downstream}$ = fan downstream pressure loss
P_{zone} = zone pressure
P_{comp} = compressor power
P_{fan} = fan power
SHR = sensible heat ratio
$Stage$ = compressor stage number
$T_{air,db,evap}$ = dry-bulb temperature of air entering evaporator

$T_{air,wb,evap}$ = wet-bulb temperature of air entering evaporator
T_{cond} = condensing temperature
T_{evap} = evaporating temperature
T_{sc} = subcooling temperature
T_{sh} = superheat temperature
T_{sup} = supply air temperature
UA = combined heat transfer coefficient
V = supply air volumetric flow rate
RH = air relative humidity
h_{air} = air enthalpy
m_{air} = supply air mass flow rate
$m_{cond,air}$ = air mass flow rate across condenser
m_r = refrigerant mass flow rate
q_{cond} = condenser capacity
q_{sen} = evaporator sensible capacity
$q_{sen,req}$ = required sensible capacity
q_{tot} = evaporator total capacity

Subscript
DX = DX unit related variables
max = variable upper bound
min = variable lower bound
setpoint = control variable setpoint
zone = zone related variables